AMERICAN SOCIETY FOR MICROBIOLOGY | Applied and Environmental Microbiology®

BIOTECHNOLOGY

Imposed Environmental Stresses Facilitate Cell-Free Nanoparticle Formation by *Deinococcus radiodurans*

Angela Chen, Lydia M. Contreras, Benjamin K. Keitz

McKetta Department of Chemical Engineering, University of Texas at Austin, Austin, Texas, USA

ABSTRACT The biological synthesis of metal nanoparticles has been examined in a wide range of organisms, due to increased interest in green synthesis and environmental remediation applications involving heavy metal ion contamination. *Deinococcus radiodurans* is particularly attractive for environmental remediation involving metal reduction, due to its high levels of resistance to radiation and other environmental stresses. However, few studies have thoroughly examined the relationships between environmental stresses and the resulting effects on nanoparticle biosynthesis. In this work, we demonstrate cell-free nanoparticle production and study the effects of metal stressor concentrations and identity, temperature, pH, and oxygenation on the production of extracellular silver nanoparticles by *D. radiodurans* R1. We also report the synthesis of bimetallic silver and gold nanoparticles following the addition of a metal stressor (silver or gold), highlighting how production of these particles is enabled through the application of environmental stresses. Additionally, we found that both the morphology and size of monometallic and bimetallic nanoparticles were dependent on the environmental stresses imposed on the cells. The nanoparticles produced by *D. radiodurans* exhibited antimicrobial activity comparable to that of pure silver nanoparticles and displayed catalytic activity comparable to that of pure gold nanoparticles. Overall, we demonstrate that biosynthesized nanoparticle properties can be partially controlled through the tuning of applied environmental stresses, and we provide insight into how their application may affect nanoparticle production in *D. radiodurans* during bioremediation.

IMPORTANCE Biosynthetic production of nanoparticles has recently gained prominence as a solution to rising concerns regarding increased bacterial resistance to antibiotics and a desire for environmentally friendly methods of bioremediation and chemical synthesis. To date, a range of organisms have been utilized for nanoparticle formation. The extremophile *D. radiodurans*, which can withstand significant environmental stresses and therefore is more robust for metal reduction applications, has yet to be exploited for this purpose. Thus, this work improves our understanding of the impact of environmental stresses on biogenic nanoparticle morphology and composition during metal reduction processes in this organism. This work also contributes to enhancing the controlled synthesis of nanoparticles with specific attributes and functions using biological systems.

KEYWORDS *Deinococcus*, environmental stress, extremophile, nanoparticles

Received 5 April 2017 **Accepted** 22 June 2017

Accepted manuscript posted online 7 July 2017

Citation Chen A, Contreras LM, Keitz BK. 2017. Imposed environmental stresses facilitate cell-free nanoparticle formation by *Deinococcus radiodurans*. Appl Environ Microbiol 83:e00798-17. https://doi.org/10.1128/AEM.00798-17.

Editor Shuang-Jiang Liu, Chinese Academy of Sciences

Address correspondence to Lydia M. Contreras, lcontrer@utexas.edu, or Benjamin K. Keitz, keitz@utexas.edu.

Mining and other industrial processes produce significant amounts of metal-ion-contaminated waste streams, necessitating water remediation efforts (1, 2). One attractive method for remediation is the use of microorganisms with the ability to degrade organic pollutants into less toxic species or to reduce metal ions to their solid metal forms via nanoparticle (NP) formation, as these organisms can be genetically engineered for improved pollutant binding and reducing capabilities (3–5). In addition

to environmental remediation, biosynthesized nanoparticles can be used in commercial applications ranging from medicine to electronics, due to their antimicrobial and catalytic properties (6, 7). For example, it has been shown that, when used in tandem with traditional antibiotics, silver nanoparticles can enhance the overall antimicrobial effect, supporting their potential as antibiotic supplements or replacements (8, 9). Similarly, metal nanoparticles can act as catalysts for a variety of useful reactions (10–12).

Members of several phyla, including archaea, plants, fungi, and bacteria, have demonstrated an ability to form nanoparticles composed of a variety of different metals; some include silver, gold, and palladium (13–16). Relative to these organisms, extremophiles offer a unique advantage for nanoparticle production and environmental remediation due to their greater tolerance for extreme conditions and their potential for more robust nanoparticle-capping ligands and proteins (17). Already, many extremophiles play key roles in the biogeochemical cycling and bioremediation of numerous minerals and metals (18).

One of the most studied extremophiles, *Deinococcus radiodurans*, is a Gram-positive bacterium possessing extremely high tolerances to radiation, desiccation, and other environmental stresses; these attributes have sparked significant interest in this organism for applications in bioremediation and metal detoxification (19–21). Indeed, *D. radiodurans* has been engineered for use in radioactive waste manipulation through incorporation of heterologous genes for toluene degradation and mercury and uranium reduction, demonstrating the ability for simultaneous reduction of multiple wastes (22, 23). These characteristics and applications demonstrate the potential of *D. radiodurans* as an ideal species for both environmental remediation and the biosynthetic production of nanoparticles.

Despite its exploration for related bioremediation purposes, few studies have examined the ability of wild-type *D. radiodurans* to form metal nanoparticles (24, 25). Furthermore, those studies and others focused primarily on monometallic nanoparticle formation, despite the increased diversity of applications and the advantages of bimetallic or multimetallic particles. The impact of acute environmental stresses on nanoparticle formation and the potential for cell-free nanoparticle production were not investigated in those studies despite analogous work with other organisms (26, 27). This raises the questions of whether cell-free supernatants from *D. radiodurans* can be equally effective for metal nanoparticle production and what impact environmental stresses may have on the diversity of nanoparticles produced in this process.

Several studies have suggested that environmental factors such as growth phase, pH changes, and exposure to metal ions can significantly affect the biological production of nanoparticles by inducing defensive stress response mechanisms; this has now been demonstrated in studies of *Bacillus licheniformis* and *Escherichia coli* (27–31). Given our understanding that environmental stresses can have significant effects on protein and gene expression in *D. radiodurans*, it is rational to suspect that a complex interplay exists between environmental stresses and nanoparticle properties and production (32, 33). Understanding (and ultimately controlling) how different processing and metabolic stresses affect nanoparticle properties when they are produced in any biological host is highly relevant to both bioremediation and biosynthesis applications.

In this work, we investigated how environmental stresses affect the properties of biogenic inorganic materials generated by *D. radiodurans*. We systematically tested experimental and culture conditions, such as temperature, pH, and oxygenation, and identified optimal conditions for improved silver nanoparticle yield. Our results demonstrate that the cell-free synthesis of silver and bimetallic (silver and gold) nanoparticles in *D. radiodurans* is facilitated by the addition of a metal environmental stressor. We also show that tuning the environmental stressors provides control over nanoparticle morphology, composition, and size. Lastly, we demonstrate the ability of bimetallic nanoparticles produced from *D. radiodurans* to acquire combinatorial properties of both pure silver and pure gold nanoparticles, including antibacterial and catalytic activities. Collectively, our results provide insight into the effects of environmental

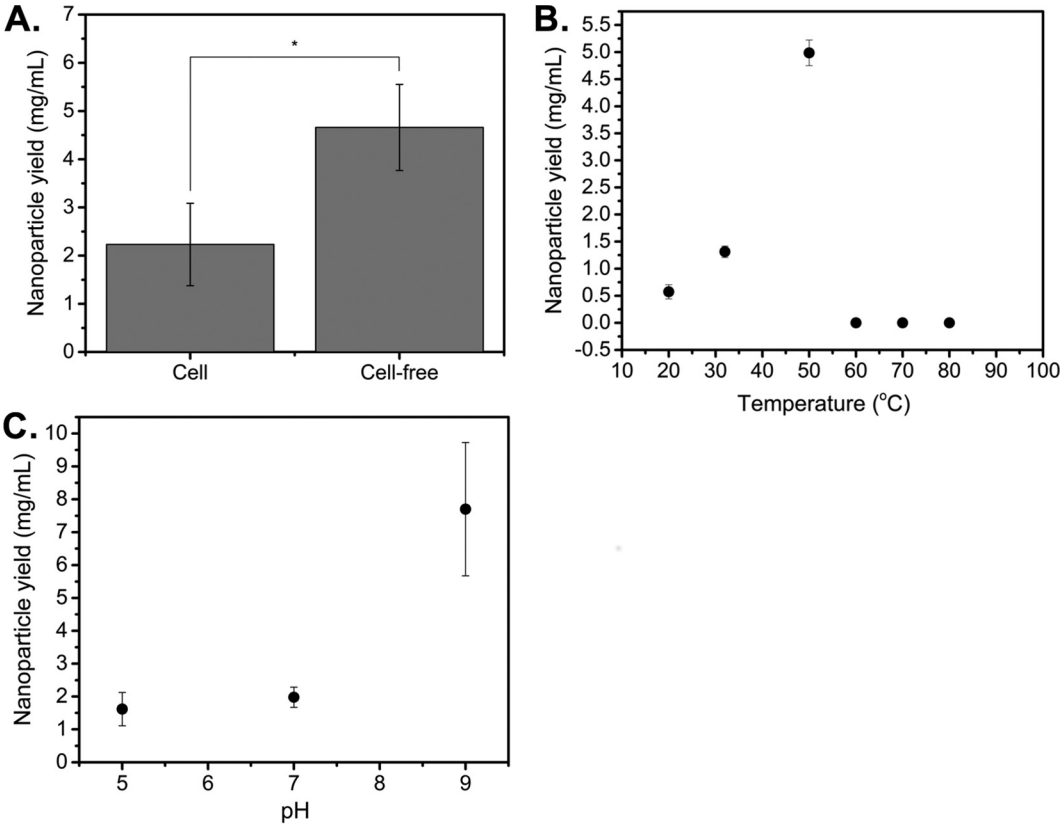

FIG 1 Screening of culturing and reaction conditions reveals that cell-free reduction and reaction temperatures up to 50°C improve nanoparticle yield. (A) Silver nanoparticle yield data using isolated cell-free supernatants from stationary-phase cultures, compared to cell-mediated production, after addition of 5 mM $AgNO_3$ at 32°C. *, $P < 0.05$, significant by Student's *t* test. (B) Comparison of cell-free nanoparticle yields after addition of 5 mM $AgNO_3$ at different reaction temperatures. (C) Effect of pH on silver nanoparticle yield. The supernatant was adjusted to different pH values and incubated for 2 h before isolation of the supernatant and addition of 5 mM $AgNO_3$. Data represent the mean ± standard deviation of three replicates.

stresses on nanoparticle production and properties and support the use of *D. radiodurans* in environmental remediation as a versatile organism for the controlled production of nanoparticles.

RESULTS

Cell-free reduction improves silver nanoparticle production. Given that previous studies in *D. radiodurans* demonstrated cell-mediated reduction only, we sought to test whether *D. radiodurans* supernatant could also facilitate nanoparticle production. We first examined the effect of cell-free supernatants on nanoparticle yields, compared to cell-mediated levels. All experiments were performed using stationary-phase cells, as our analysis of the effect of growth phase on nanoparticle production by *D. radiodurans* showed no significant effect when results were normalized on the basis of optical density (OD) values (see Fig. S1A in the supplemental material). Cells were grown to stationary phase, and $AgNO_3$ was added either to the isolated cell-free supernatant or directly to the culture (for cell-mediated experiments) and was reacted for 48 h. Nanoparticle production was observed under both conditions, as indicated by peaks at ~426 nm in the UV-visible (UV-vis) absorption spectrum, demonstrating that cell-free synthesis of silver nanoparticles using *D. radiodurans* supernatant was possible. The presence of a peak at ~426 nm also confirmed that the silver nanoparticles were elemental silver and not silver oxides, which exhibit a characteristic maximum near 650 nm (34). Uninoculated tryptone-glucose-yeast (TGY) medium was treated with $AgNO_3$ as a control, to ensure that silver reduction was exclusively due to cellular reducing factors, and it showed no evidence of nanoparticle formation. As shown in Fig. 1A,

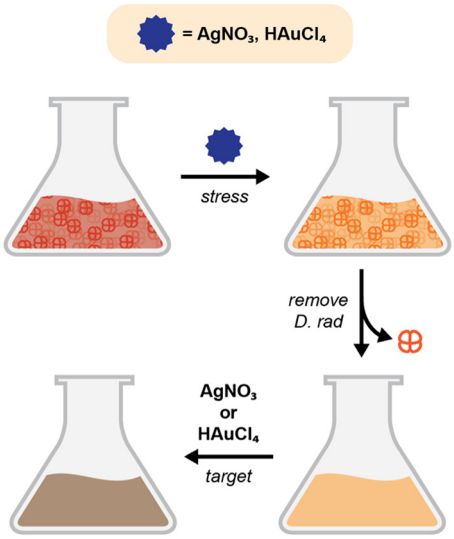

FIG 2 Experimental scheme of the nanoparticle production process using an environmental stressor. Cells are cultured to stationary phase before being stressed with the environmental stressor for 2 h. The cell-free supernatant is then isolated, the metal target (5 mM $AgNO_3$ or 1 mM $HAuCl_4$) is added, and the mixture is incubated for 48 h.

cell-free reduction improved yields 2-fold (from 2.23 mg/ml to 4.66 mg/ml) and greatly simplified nanoparticle isolation. Therefore, we conducted all further experiments under cell-free conditions.

We next investigated the effects of the temperature, oxygenation, and pH of the supernatant on nanoparticle yields. These factors are known to influence nanoparticle properties such as size due to their roles in controlling reaction rates and acting as electron acceptor competitors (35, 36). Experiments were performed as described above except that the 48-h incubation temperature was varied from 20°C to 80°C or the reaction was performed at 32°C at pH 5, 7, or 9 or at pH 7 under anaerobic conditions. Improved nanoparticle yields were obtained at a maximum temperature of 50°C (4.99 mg/ml versus 1.31 mg/ml) (Fig. 1B) or under anaerobic conditions (2.04 mg/ml versus 1.42 mg/ml) (Fig. S1B), consistent with our earlier hypothesis. The effect of oxygen on nanoparticle yields was not as pronounced as expected, however, due to oxygen consumption by *D. radiodurans* during the course of the reduction. Nanoparticle reduction was measured at all pH values, and the yields were found to increase with increasing basicity of the culture, with a shift from 1.98 mg/ml to 7.70 mg/ml when the pH was increased from 7 to 9 (Fig. 1C). This trend of basic conditions promoting nanoparticle production is consistent with studies with other organisms (29, 37). Importantly, these results suggest that reaction temperature, pH, and oxygenation levels can be optimized for modest improvements in silver nanoparticle yields. Lastly, since we observed an effect on yield, we examined the effect of temperature on nanoparticle morphology, but we found no statistical difference in nanoparticle size with increasing reduction temperatures up to 50°C (Fig. S1C). Due to the technical challenge of performing anaerobic reduction, all further experiments were conducted under aerobic conditions only.

The addition of an environmental stressor affects silver nanoparticle production and morphology. After optimizing cell-free nanoparticle synthesis conditions as described above, we adopted an experimental scheme (outlined in Fig. 2) that incorporated environmental stressors in the production of nanoparticles using *D. radiodurans* supernatant. Cells were grown to stationary phase and then exposed to an environmental stressor for 2 h. We hypothesized that stress would induce a response that could favor nanoparticle production, given that the synthesis of nanoparticles is likely a defense mechanism initiated to reduce the abundance of toxic metal ions in the

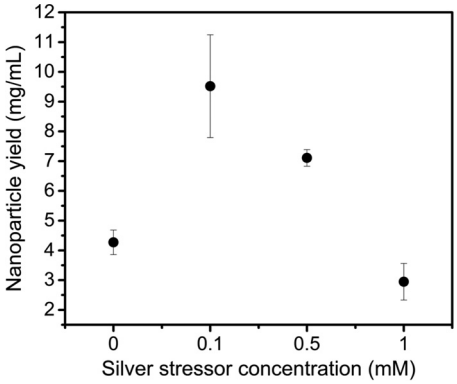

FIG 3 Effects of environmental stressors on silver nanoparticle yield show that addition of up to 1 mM $AgNO_3$ improves nanoparticle yield. Cells were stressed with different concentrations of $AgNO_3$ before isolation of the supernatant and addition of 5 mM $AgNO_3$. Data represent the mean ± standard deviation of three replicates.

environment. We examined exposure to a metal solution (0.1 to 1 mM $AgNO_3$ or $HAuCl_4$), because bioremediation sites are typically contaminated with numerous metal species (1). The cell-free supernatant was subsequently isolated and reacted with the metal target, which consisted of a higher concentration of metal (5 mM $AgNO_3$ or 1 mM $HAuCl_4$). All nanoparticles produced using a metal stressor are identified as "metal stressor-metal target NPs." For example, nanoparticles produced using silver stress and silver as a metal target are Ag-AgNPs.

We tested the effect of the initial silver stress concentration on silver nanoparticle yield, since we reasoned that silver, which is noted for its toxicity against bacteria, would be ideal for inducing a stress response and promoting the reduction of toxic metals. As shown in Fig. 3, increases in nanoparticle yield were observed for all $AgNO_3$ concentrations except 1 mM $AgNO_3$, relative to the no-stress condition. We attribute the reduction in yield at 1 mM $AgNO_3$ to cell death caused by the antimicrobial effects of silver at that concentration. Collectively, these results indicate that environmental stresses can influence silver nanoparticle yield.

After studying the effects of environmental stressors on particle yields, we sought to characterize their effects on the morphology and size distribution of Ag-AgNPs, since these properties govern nanoparticle application and function. Our previous results showed that pH had a negligible effect on particle size; therefore, we focused only on silver stress. The nanoparticle size was calculated using only spherical particles in each population. A representative bright-field transmission electron microscopy (TEM) image of the resulting Ag-AgNPs, which appear similar to other biologically and commercially produced silver nanoparticles, is shown in Fig. 4A. Interestingly, increasing the initial $AgNO_3$ stress concentration (0, 0.1, 0.5, or 1 mM) resulted in increased morphological homogeneity of the resulting Ag-AgNPs (Fig. S2A and B) and a reduction in particle size (from 56 ± 17.2 nm to 25 ± 8.5 nm) (Fig. 4B), consistent with a blue shift of the absorbance peaks (Fig. S1D). Due to the polydispersity of the nanoparticles, the measured reduction in nanoparticle size with 0.1 mM or 0.5 mM $AgNO_3$ was negligible.

Metal stressors enable bimetallic nanoparticle formation. To explore the possibility of synthesizing different types of NPs (other than Ag-AgNPs) in *D. radiodurans*, we screened copper, iron, and gold as reduction targets, following the scheme outlined in Fig. 2. However, only gold was found to produce bimetallic nanoparticles in cases in which silver was also in the system (as either the initial stressor or the target). We observed no nanoparticle formation when we tested iron or copper alone and no bimetallic nanoparticles, even in the presence of silver. Importantly, we were unable to observe cell-free gold reduction in the absence of silver stress, which indicates that *D. radiodurans* requires the presence of a silver stress to seed cell-free gold reduction.

The use of silver as a metal stressor results in the formation of Ag-AuNPs that exhibit size and morphological sensitivity to the silver stress concentration. For

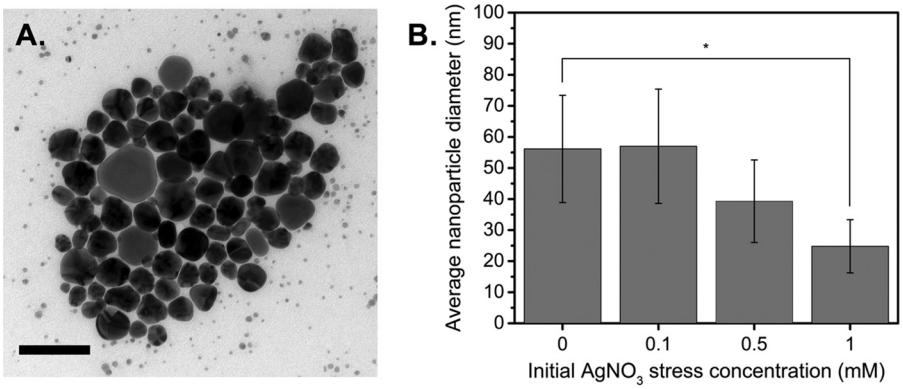

FIG 4 Silver stress influences nanoparticle yield and properties. (A) Representative bright-field TEM image of Ag-AgNPs (scale bar, 100 nm). (B) Size distribution of Ag-AgNPs produced using different $AgNO_3$ stressor concentrations with a metal target of 5 mM $AgNO_3$. Size distribution was calculated from TEM images using ImageJ software. Data represent the mean ± standard deviation of three replicates. *, $P < 0.05$.

these experiments, *D. radiodurans* was treated with various concentrations of $AgNO_3$ as an initial stress and the supernatant was exposed to $HAuCl_4$ as a metal target. Elemental mapping analysis of the Ag-AuNPs (Fig. 5A) confirmed the bimetallic nature of the nanoparticles, with an elemental composition of 73% gold and 27% silver being determined via energy-dispersive X-ray spectroscopy (EDXS) data, reflecting the fact that $HAuCl_4$ was in excess in a 2:1 ratio. This was further supported by the deep purple-black color of the supernatant and the appearance of a single absorption peak at ~546 nm in the UV-vis spectrum (Fig. S3A). Bright-field TEM images (Fig. S3B and C) illustrate the unique morphology of the Ag-AuNPs and demonstrate how different concentrations of silver stressor drastically affected nanoparticle morphology. Similar to the Ag-AgNPs, we observed a decrease in nanoparticle size with increasing $AgNO_3$ stress (Fig. 5B). These results show that using silver as the initial stressor enables the formation of bimetallic Ag-AuNPs and influences morphology. Collectively, these findings raise the strong possibility that silver may be acting as a nucleation seed for gold. Our results also highlight the importance of metal stressors in nanoparticle production, as previous work (in the absence of such stressors) (25) showed no evidence of cell-free gold nanoparticle formation. Thus, we hypothesize that gold reduction by *D. radiodurans* is likely intracellular but cell-free reduction can be enabled under specific conditions, such as the presence of a silver stressor.

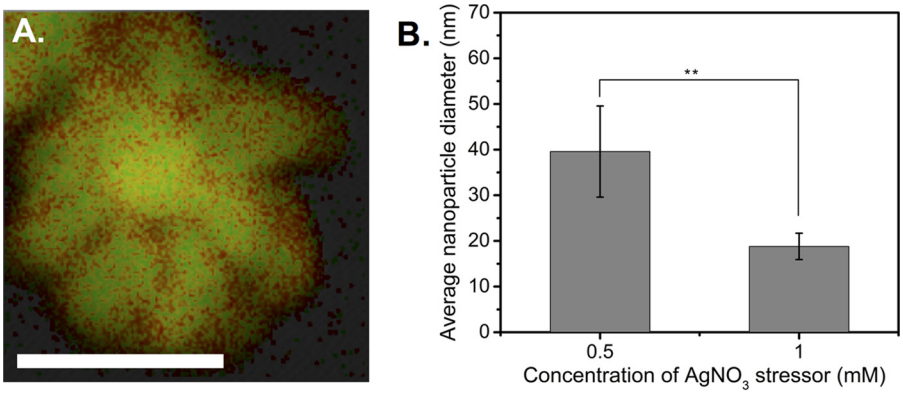

FIG 5 Use of silver as a metal stressor results in primed reduction of gold into bimetallic nanoparticles. (A) Elemental mapping data for an Ag-AuNP; red represents silver, green represents gold, and yellow indicates the presence of both metals (scale bar, 25 nm). (B) Size distribution data for Ag-AuNPs synthesized using different $AgNO_3$ stress concentrations. Data represent the mean ± standard deviation of three replicates. **, $P < 0.01$.

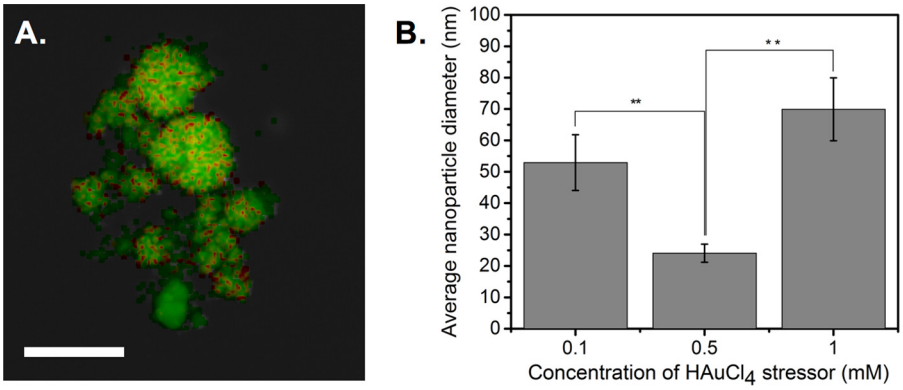

FIG 6 Use of gold as a metal stressor alters the composition and size distribution of bimetallic nanoparticles. (A) Elemental mapping data for an Au-AgNP; red represents gold, green represents silver, and yellow indicates the presence of both metals (scale bar, 100 nm). (B) Size distribution data for Au-AgNPs synthesized using different $HAuCl_4$ stress concentrations. Data represent the mean ± standard deviation of three replicates. **, $P < 0.01$.

The use of gold as a metal stressor results in the formation of Au-AgNPs that exhibit size and morphological sensitivity to the gold stress concentration. To explore the potential for further increasing the diversity of the synthesized bimetallic (silver-gold) nanoparticles, we switched the roles of silver and gold by using gold as an initial metal stressor and silver as the metal target. The bimetallic nature of the nanoparticles was confirmed through UV-vis spectroscopy (Fig. S4) and elemental mapping analysis of the Au-AgNPs (Fig. 6A), which revealed an elemental composition of 72% silver and 28% gold, reflecting the fact that $AgNO_3$ was in excess in a 5:1 ratio. Bright-field TEM images (Fig. S4B to D) demonstrate how different concentrations of gold stressor greatly affect nanoparticle morphology and consequently the size distribution of the Au-AgNPs (Fig. 6B). Specifically, the average size of the Au-AgNPs decreased (from 53 ± 10 nm to 24 ± 2.9 nm) and then increased (from 24 ± 2.9 nm to 70 ± 10 nm) as the concentration of $HAuCl_4$ was varied from 0.1 mM to 0.5 mM to 1 mM. These trends are likely due to the appearance of a population of intermediate nanoparticles at 0.5 mM $HAuCl_4$ (Fig. S4C), similar to the intermediates observed in Fig. S3C. Elemental data for these populations confirmed their silver and gold composition (Fig. S4E). Thus, the addition of environmental stresses (specifically metals) enables cell-free production of bimetallic nanoparticles with unique compositions and morphologies, which were previously inaccessible with traditional methods.

Antimicrobial and catalytic studies of the biosynthetic nanoparticles show that bimetallic nanoparticles have the combined properties of monometallic nanoparticles. Given the interest in using nanoparticles for applications involving antimicrobial function, we next evaluated the antimicrobial activity of our nanoparticles against *D. radiodurans* (Gram-positive bacterium) and *E. coli* (Gram-negative bacterium). As shown in Fig. 7A, Ag-AgNPs produced under a range of environmental stresses exhibited antimicrobial activity against both bacteria, consistent with observations for other biosynthetic silver nanoparticles (24, 38). Interestingly, the Au-AgNPs demonstrated activity similar to that of the Ag-AgNPs, while the Ag-AuNPs exhibited substantially diminished antimicrobial activity. This phenomenon is consistent with results for other organisms, suggesting that the antimicrobial activity of bimetallic nanoparticles may be directly correlated with the amount of silver present in the nanoparticles (39). The MICs for *D. radiodurans* and *E. coli* were obtained from microtiter dilution curves (Fig. S5A and B). The MIC value for the Ag-AgNPs and Au-AgNPs against *E. coli* was approximately 10-fold greater than that for *D. radiodurans* (128 μg/ml versus 16 μg/ml), demonstrating a wide range of toxicities against different bacteria. Surprisingly, the Ag-AuNPs demonstrated much higher MIC values for *E. coli* and *D. radiodurans* (>512 μg/ml and >125 μg/ml, respectively), supporting earlier observations that the Ag-AuNPs have reduced antimicrobial activity. Furthermore, only the Ag-AuNPs produced with the

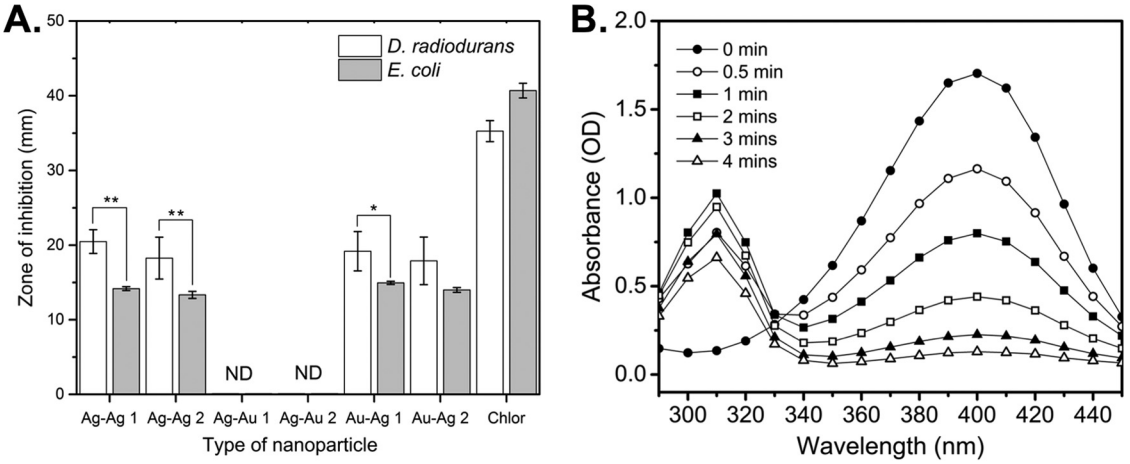

FIG 7 Antimicrobial and catalytic assays reveal that bimetallic nanoparticles have the combined functions of their monometallic counterparts. (A) Average zone-of-inhibition data for Ag-AgNPs and Au-AgNPs from agar well diffusion assays with *D. radiodurans* and *E. coli*. Each well contained 40 μg of nanoparticles, and chloramphenicol (10 μg for *D. radiodurans* and 25 μg for *E. coli*) was used as a positive control. 1 and 2 denote addition of 0.1 mM metal stressor and 1 mM metal stressor, respectively. A zone of inhibition was not detected (ND) for either bacterium after treatment with 40 μg of Ag-AuNP 1 or Ag-AuNP 2. (B) Time-dependent UV-vis spectra for the catalytic reduction of 4-NP by $NaBH_4$ in the presence of Ag-AuNPs. Data represent the mean $\pm$ standard deviation of three replicates. **, $P < 0.01$; *, $P < 0.05$.

highest silver stress concentration (1 mM) showed any antimicrobial activity. Despite the drastic size and morphological differences observed between the Ag-AgNPs and the Au-AgNPs when they were produced under different environmental stresses, there was little difference in their antimicrobial behavior. This observation demonstrated that the addition of gold did not diminish the antimicrobial activity of the primarily silver Au-AgNPs.

While silver is noted for its antimicrobial properties, gold has commonly been associated with catalysis and imaging (40, 41). To illustrate the potential of the bimetallic nanoparticles to retain properties typical of pure gold nanoparticles, we tested their ability to catalyze the reduction of 4-nitrophenol (4-NP) to 4-aminophenol (4-AP). As shown in Fig. 7B, the Ag-AuNPs demonstrated the ability to catalyze 4-NP reduction, as evidenced by the decrease in absorbance at 400 nm (corresponding to the 4-nitrophenolate ion) and the increase in absorbance at 310 nm (corresponding to 4-AP) over time. The rate constants for the reduction were calculated for the Ag-AgNPs and the bimetallic nanoparticles by using linear fits of the absorbance at 400 nm over time (Fig. S6), and they were found to be consistent with previous literature reports (Table 1). It is worthwhile to note that the rate constants for the Ag-AuNPs and Au-AgNPs were greater than that for pure silver and consistent with that for pure gold, illustrating how the bimetallic nanoparticles have improved and combinatorial properties, compared to their monometallic counterparts. Additionally, we observed greater rate constants with increased gold percentages or decreased nanoparticle size within

TABLE 1 Comparison of results with different types of nanoparticles

Nanoparticle type[a]	Calculated rate constant (10^{-3} s^{-1})
Ag-AgNP, 0.1 mM metal stressor (this study)	7.42 $\pm$ 2.36
Ag-AgNP, 1 mM metal stressor (this study)	10.63 $\pm$ 3.74
Ag-AuNP, 0.1 mM metal stressor (this study)	13.70 $\pm$ 6.07
Ag-AuNP, 1 mM metal stressor (this study)	12.91 $\pm$ 3.05
Au-AgNP, 0.1 mM metal stressor (this study)[b]	15.23 $\pm$ 6.13
Au-AgNP, 1 mM metal stressor (this study)[b]	23.85 $\pm$ 4.57
AuNP, chemically synthesized	12.12 $\pm$ 1.85
AuNP (53)	1.86
AgNP (58)	1.23

[a]Linear fits for each nanoparticle type can be found in Fig. S6 in the supplemental material.
[b]The linear fit was less than $R^2 = 0.95$ because the data did not fit pseudo-first-order kinetics well.

a single nanoparticle type. These results indicate that the bimetallic nanoparticles retain properties of both base metals, allowing fusion of multiple functionalities in a single particle.

DISCUSSION

We identified several trends in this work while investigating factors that contribute to optimizing nanoparticle synthesis by *D. radiodurans*. First, our investigations of the optimal culture conditions for silver nanoparticle production in *D. radiodurans* revealed that the more convenient cell-free synthesis (using stationary-phase supernatant) led to substantial increases in nanoparticle yield. The capability for cell-free synthesis is consistent with previous reports showing that supernatants from *D. radiodurans* could protect other organisms from oxidative stress, and it provides further evidence for secreted reducing factors or other extracellular redox machinery that may play a role in nanoparticle synthesis (42). Interestingly, we also noticed that the beneficial effect of cell-free synthesis on nanoparticle yield was ablated with increasing metal stress concentrations (see Fig. S7 in the supplemental material). We suspect that this observation is due to increased cell toxicity at higher metal concentrations and, consequently, decreased amounts of reducing factors present in the supernatant.

Second, our results demonstrate that chemical optimization, particularly regarding oxygen levels, alkalinity, and temperature (up to a limit of 50°C), can affect nanoparticle yields. Taken together, these results suggest that enzymes or proteins that degrade at high temperatures may be mediating the reduction process. Reports with similar observations using other organisms have implicated nitrate reductase as being crucial for silver nanoparticle formation (29, 43). The role of a reductase is further supported by studies showing that the reducing power of this protein is enhanced under alkaline conditions, as alkaline ions are needed for metal ion reduction, and by the fact that nitrate reductase has been identified in numerous reports of extracellular silver nanoparticle synthesis (29, 44). A NADH-dependent reductase was also implicated in the synthesis of gold and silver nanoparticles by an anaerobic consortium (45). While there is no annotated nitrate reductase in *D. radiodurans*, it is possible that the silver reduction mechanism could be facilitated by similar enzymes.

Third, we report that *D. radiodurans* is capable of producing bimetallic nanoparticles composed of gold and silver, through the introduction of a metal environmental stress. These bimetallic nanoparticles are elemental in nature, as evidenced by only a trace peak for oxygen in the EDXS data, which is likely due to the presence of proteins or carbohydrates that act as capping ligands. Importantly, throughout our studies, we were able to reduce gold extracellularly only in the presence of silver, suggesting that silver acts as a nucleation seed for gold. We did not observe core-shell nanoparticles, however, but we observed alloys of silver and gold, despite the temporal differences in gold and silver addition. This phenomenon could be attributed to spontaneous galvanic displacement, with the more noble metal (gold) displacing electrons from the less noble metal (silver), as this was demonstrated previously with triangular nanoplates of silver that could be used as sacrificial templates for gold nanorings (46). Thus, one potential mechanism for Ag-AuNP formation is silver cycling, in which the initial silver nanoparticles are reverted back to free Ag^{+} ions through loss of electrons to Au^{3+}, enabling formation of gold nanoparticles. The free Ag^{+} ions are then reduced again, and the silver nanoparticles are reformed in conjunction with the gold nanoparticles.

Lastly, we demonstrated that the morphology and composition of nanoparticles produced by *D. radiodurans* can be controlled through changes in the stressor and target metal identities and tuning of the stressor and target metal concentrations. Use of a silver metal stressor improved nanoparticle yield and affected nanoparticle morphology, as evidenced by the decreased nanoparticle size and increased nanoparticle homogeneity with increasing silver stressor concentrations. These results are similar to observations of platinum nanoparticle formation by a bacterial consortium, in which increased nanoparticle homogeneity was seen with increased platinum concentrations, and are consistent with studies showing that silver nanoparticles decreased in size with

increasing metal concentrations or decreasing leaf broth concentrations (47, 48). Thus, it may be that, at higher metal concentrations, the ratio of reducing factors to metal substrate is lower, limiting nanoparticle aggregation by secondary reduction events on preformed particles and favoring nucleation of new particles.

With respect to the Ag-AuNPs, we observed that modulation of the metal stressor concentration dramatically affected nanoparticle size and shape (Fig. S3B and C). A similar stress-concentration-dependent size phenomenon was observed with the Au-AgNPs, as evidenced by the average nanoparticle size (Fig. 6B). As the molar ratio of gold to silver was increased from 1:50 to 1:10 and 1:5, the nanoparticle size, composition, and morphology evolved from being reminiscent of pure silver nanoparticles to representing the jagged spherical nanoparticles observed in Fig. S4D. These results suggest that, at 1:1 or similar ratios of silver and gold, there is significant competition between the two metals for reducing factors, which favors the production of many small monometallic and bimetallic nanoparticles rather than the growth of a few large bimetallic nanoparticles. This hypothesis is supported by elemental composition data for the intermediate particles shown in Fig. S4C, which reveal that the nanoparticle population is composed of small pure gold nanoparticles mixed with small gold and silver alloy nanoparticles (Fig. S4E). Unlike observations at other molar ratios (Fig. S4B and D), which indicated only large bimetallic nanoparticles, the intermediate particles illustrate how the balance between nucleation of new particles and growth on preformed nanoparticle seeds that exists at these ratios results in drastically reduced nanoparticle sizes. However, since the reduction mechanisms of *D. radiodurans* are still unknown, further experiments are required to fully elucidate the mechanisms though which environmental stressor conditions govern nanoparticle formation and morphology.

Examination of the properties of the bimetallic nanoparticles revealed antimicrobial activity against *E. coli* and *D. radiodurans*. Moreover, we observed that differences in nanoparticle composition and morphology could greatly affect the properties and applications of nanoparticles. Previous studies showed increased microbial inhibition with decreased nanoparticle size but, surprisingly, we did not observe any significant differences in antimicrobial activity due to nanoparticle size (49). However, the size range of our nanoparticles was relatively small (20 to 70 nm). Alternatively, these results could be attributed to the various mechanisms by which silver and silver-containing nanoparticles are toxic. Although AgNPs have been identified within the nuclei of cells as potential DNA-damaging agents, others have suggested the release of Ag^+ and the subsequent production of reactive oxygen species as the primary mechanism for cell death (50). The latter mechanism is consistent with our observations that Ag-AgNPs and Au-AgNPs demonstrated increased antimicrobial activity, compared to Ag-AuNPs, as the former contain approximately the same amounts of silver and are similar in antimicrobial activity. Furthermore, the fact that only Ag-AuNPs produced with the highest concentration of silver stress exhibited any antimicrobial activity, despite their unique morphology, lends further support for the toxic release of Ag^+ (51). Overall, our observations are consistent with other studies that suggest that the incorporation of gold, especially a high percentage of gold, decreases the concentration of silver and significantly reduces the toxicity of the bimetallic nanoparticles (50).

We also evaluated the catalytic ability of the biosynthetic nanoparticles to reduce 4-NP, a common wastewater pollutant due to its frequent use in the textile, paint, and paper industries, to 4-AP (52). Although the reduction is thermodynamically favored, the nanoparticles act as electron shuttles from BH_4^- to 4-NP, reducing the kinetic barrier caused by the large potential difference between the two species (53). As seen in Fig. 7B, use of the bimetallic nanoparticles as catalysts enables reaction completion within 5 min, which is faster than with other biosynthetic or chemically synthesized nanoparticles (53). Comparison of the calculated rate constants for our biosynthetic nanoparticles with literature values for other biosynthetically or chemically synthesized nanoparticles (Table 1) illustrates that our nanoparticles display catalytic activity comparable to that of other nanoparticles. Interestingly, we also

noted a distinct lag phase for the Ag-AgNPs and Ag-AuNPs but not the Au-AgNPs, which may be due to the large proportion of silver present and its relative location in the Ag-AuNPs and Ag-AgNPs, compared to the Au-AgNPs. Silver typically forms larger nanoparticles and is easily oxidized, reducing its catalytic activity, which explains the significantly lower rate constants for our Ag-AgNPs, compared to the bimetallic nanoparticles (54). A previously reported observation supports this claim, as substantially smaller silver nanoparticles (particle radius, 3 nm) were shown to exhibit catalytic activity on the order of $k = 15.46 \times 10^{-3}\ s^{-1}$ (55).

In this work, we showed that *D. radiodurans* is capable of producing monometallic and bimetallic nanoparticles in a cell-free manner and that nanoparticle production can be optimized through tuning of culture, processing, and environmental stress conditions. The bimetallic nanoparticles retained antimicrobial and catalytic activities, illustrating how the use of an environmental stressor during nanoparticle biosynthesis enables production of nanoparticles that possess dual-metal functionality in a single particle. Furthermore, the ability to produce bimetallic nanoparticles via reduction of multiple metal species strengthens the application of *D. radiodurans* in bioremediation, as many environmentally hazardous areas are contaminated with multiple metals and organic pollutants. These results further support the potential of *D. radiodurans* for applications in bioremediation and precious metal recovery, while providing insight into how environmental stresses influence the properties of biosynthetic nanoparticles.

MATERIALS AND METHODS

Bacterial strains and growth conditions. *Deinococcus radiodurans* strain R1 (ATCC 13939) was grown aerobically on TGY agar plates (1% Bacto tryptone, 0.5% yeast extract, 0.2% glucose, and 1.5% Bacto agar) at 32°C and then in liquid TGY broth (1% Bacto tryptone, 0.5% yeast extract, and 0.2% glucose) at 32°C and 180 rpm, unless otherwise stated, for the nanoparticle and antimicrobial studies. For the antimicrobial studies, *Escherichia coli* DH5α was grown on Luria-Bertani (LB) agar plates (1.5% Bacto agar) at 37°C for 18 h and in LB medium at 37°C and 180 rpm. Bacterial growth was assessed by measuring the turbidity of the cultures using the optical density at 600 nm (OD_{600}). Aqueous solutions (100 mM) of $AgNO_3$ and $HAuCl_4$ (Sigma-Aldrich) were produced by dissolving the corresponding metal powders in Milli-Q water and filter sterilizing the resulting solutions.

Metal nanoparticle production. For silver nanoparticle production in the absence of stressor, *D. radiodurans* R1 was grown overnight in TGY medium at 32°C and 180 rpm. Fresh TGY medium was then inoculated to a starting OD_{600} value of ~0.2, and the culture was grown to stationary phase (OD_{600} value of ~2). After cells reached stationary phase, the supernatant was isolated via centrifugation at 2,800 × *g* for 10 min and syringe filtered using a 0.22-μm polyethylene glycol (PEG) filter. $AgNO_3$ (100 mM) was then added to the cell-free supernatant to a final concentration of 5 mM, and the supernatant was incubated for 48 h at 32°C and 180 rpm. (i) Cell-mediated production was tested by excluding the supernatant isolation step and then following the rest of the procedure using the cell culture. (ii) The effect of growth phase on silver nanoparticle production was examined by following the procedure described above except that cultures were grown to either exponential phase (OD_{600} of ~0.7) or stationary phase (OD_{600} of ~2) before the supernatant was isolated. (iii) Temperature dependence experiments were performed by adjusting the 48-h incubation temperature from 32°C to a range of temperatures (20°C, 50°C, 60°C, 70°C, or 80°C). (iv) For anaerobic experiments, the procedure described above was followed except that, after the addition of 5 mM $AgNO_3$, the cell-free supernatant was purged with argon gas for 10 min to remove any oxygen in the system before incubation. (v) For pH dependence studies, the pH of the cell-free supernatant was shifted to different values (from 5 to 9), through the addition of either aqueous 1 M NaOH or glacial acetic acid, before the addition of 5 mM $AgNO_3$. Nanoparticle production in the presence of an environmental stressor followed the standard procedure described above except that the stationary-phase cultures were stressed by the addition of an environmental stressor for 2 h before the supernatant was isolated and the metal target was added. (vi) For Ag-AgNPs, the cultures were stressed by the addition of an initial $AgNO_3$ stressor (0.1 to 1 mM $AgNO_3$). (vii) Bimetallic NP production was performed by following the silver stressor procedure but substituting the metal stressor and metal target. For Ag-AuNPs, the standard procedure was followed using silver as the metal stressor and gold as the metal target. Thus, the cell-free supernatant was treated with 100 mM $HAuCl_4$ for a final metal target concentration of 1 mM $HAuCl_4$. Similarly, Au-AgNPs were produced by changing the identity of the metal stressor to gold through the addition of various concentrations (0.1 to 1 mM) of $HAuCl_4$ while maintaining 5 mM $AgNO_3$ as the metal target.

Isolation and characterization of nanoparticles. Preliminary confirmation of nanoparticle formation was performed using UV-vis spectroscopy (Clariostar; BMG Labtech) with 100 μl of supernatant/nanoparticle suspension, using a wavelength range of 370 to 650 nm and a resolution of 2 nm. Controls of inoculated supernatant with no added metal solution and uninoculated TGY medium with the appropriate concentrations of 5 mM $AgNO_3$ or 1 mM $HAuCl_4$ were run simultaneously. Nanoparticle production was characterized by the presence of absorbance peaks corresponding to silver (~426 nm) and gold (~534 nm) (24, 56). The nanoparticles were harvested by centrifuging the nanoparticle-loaded

supernatant at 15,000 × *g* for 10 min, to separate the supernatant from the nanoparticle pellet, and then washing the pellet with Milli-Q water three times. The resulting nanoparticles were dried overnight using a vacuum centrifuge, to evaporate any remaining water. For the antimicrobial and catalytic studies, nanoparticle-loaded supernatant was combined with acetone in a 1:6 ratio and the solution was then centrifuged at 11,000 × *g* for 10 min. The resulting nanoparticle pellet was then washed twice with water/acetone at a 1:5 ratio and centrifuged at 21,000 × *g* for 3 min. The nanoparticles were dried for 1.5 h using a vacuum centrifuge, to evaporate any remaining acetone or water. After drying, the nanoparticle pellet mass was obtained. Nanoparticle solutions were created by resuspending the nanoparticle pellet in Milli-Q water. No significant aggregates were observed, which is likely due to the presence of natural capping ligands (proteins or carbohydrates); therefore, additional dispersants were unnecessary. Nanoparticle yield was determined by comparing the UV-vis absorbance peak to that of a standard with a known concentration.

Electron microscopy of nanoparticles. Carbon-coated copper grids were prepared for TEM by drop-coating the grids with the washed nanoparticle suspension. TEM images were obtained using a FEI Tecnai Spirit transmission electron microscope with an accelerating voltage of 80 kV. Lattice imaging, elemental identification, and mapping (EDXS and electron energy loss spectroscopy [EELS]) were performed using a high-resolution transmission electron microscope (JEOL 2010F) with an accelerating voltage of 200 kV, to obtain crystallinity data and to perform elemental composition analysis.

Antimicrobial assays. The antimicrobial activity of the nanoparticles was tested using agar well diffusion and microtiter broth dilution methods, as described by Balouiri et al. (57). In brief, for the agar well diffusion method, TGY and LB agar plates were spread with 100 μl of *D. radiodurans* and *E. coli*, respectively, at a concentration of 10^6 CFU/ml and were allowed to dry. Holes (diameter, 9 mm) were punched with a sterile tip and filled with 100 μl of the nanoparticle solution, for a final mass of 40 μg of nanoparticles. The plates were then incubated under suitable conditions for each organism. For the microtiter broth dilution method, the nanoparticle solutions were serially diluted 2-fold in liquid medium in a 96-well plate. Microbial inoculum was then added to each well for a final concentration of 10^5 CFU/ml, and the plate was incubated for 18 h under suitable conditions for each organism.

Catalytic assays. The catalytic activity of the nanoparticles was tested by monitoring the reduction of 4-NP to 4-AP by $NaBH_4$. Using a cuvette (path length, 10 mm), 0.8 ml of Milli-Q water was combined with 0.1 ml of aqueous 2 mM 4-NP. $NaBH_4$ was dissolved in Milli-Q water to a concentration of 200 mM, and 1 ml of this solution was then added to the cuvette, producing 4-nitrophenolate and a bright yellow color. Finally, 0.1 ml of nanoparticles (~0.2 mg/ml) was added to the cuvette and the UV-vis absorption spectrum for wavelengths ranging from 290 to 450 nm, with a resolution of 10 nm, was measured.

SUPPLEMENTAL MATERIAL

Supplemental material for this article may be found at https://doi.org/10.1128/AEM.00798-17.

SUPPLEMENTAL FILE 1, PDF file, 5.0 MB.

ACKNOWLEDGMENTS

We thank Gang Fan and Karalee Jarvis for their assistance with the high-resolution TEM and EDXS/EELS data. We gratefully acknowledge the use of facilities within the Texas Materials Institute and the core microscopy laboratory of the Institute for Cellular and Molecular Biology (University of Texas at Austin). We also acknowledge Cynthia Chu and Kierstyn Luckock for their help with the bimetallic nanoparticle studies.

This work was supported by the Air Force Office of Scientific Research Young Investigator Program (grant FA9550-16-1-0174), the Defense Threat Reduction Agency Young Investigator Program (grant HDTRA1-12-1-0016), and the Welch Foundation (grants F-1756 and F-1929). A.C. was supported by a National Science Foundation Graduate Research Fellowship (grant DGE-1610403).

REFERENCES

1. Cohen RRH. 2006. Use of microbes for cost reduction of metal removal from metals and mining industry waste streams. J Clean Prod 14:1146–1157. https://doi.org/10.1016/j.jclepro.2004.10.009.
2. Dold B. 2008. Sustainability in metal mining: from exploration, over processing to mine waste management. Rev Environ Sci Biotechnol 7:275–285. https://doi.org/10.1007/s11157-008-9142-y.
3. Löffler FE, Edwards EA. 2006. Harnessing microbial activities for environmental cleanup. Curr Opin Biotechnol 17:274–284. https://doi.org/10.1016/j.copbio.2006.05.001.
4. Singh JS, Abhilash PC, Singh HB, Singh RP, Singh DP. 2011. Genetically engineered bacteria: an emerging tool for environmental remediation and future research perspectives. Gene 480:1–9. https://doi.org/10.1016/j.gene.2011.03.001.
5. Ontiveros-Valencia A, Tang Y, Krajmalnik-Brown R, Rittmann BE. 2013. Perchlorate reduction from a highly contaminated groundwater in the presence of sulfate-reducing bacteria in a hydrogen-fed biofilm. Biotechnol Bioeng 110:3139–3147. https://doi.org/10.1002/bit.24987.
6. Hennebel T, De Gusseme B, Boon N, Verstraete W. 2009. Biogenic metals in advanced water treatment. Trends Biotechnol 27:90–98. https://doi.org/10.1016/j.tibtech.2008.11.002.
7. Edmundson MC, Capeness M, Horsfall L. 2014. Exploring the potential of metallic nanoparticles within synthetic biology. N Biotechnol 31:572–577. https://doi.org/10.1016/j.nbt.2014.03.004.
8. Rai M, Yadav A, Gade A. 2009. Silver nanoparticles as a new generation of antimicrobials. Biotechnol Adv 27:76–83. https://doi.org/10.1016/j.biotechadv.2008.09.002.

9. Fayaz AM, Balaji K, Girilal M, Yadav R, Kalaichelvan PT, Venketesan R. 2010. Biogenic synthesis of silver nanoparticles and their synergistic effect with antibiotics: a study against Gram-positive and Gram-negative bacteria. Nanomed Nanotechnol Biol Med 6:103–109. https://doi.org/10.1016/j.nano.2009.04.006.
10. Corma A, Garcia H. 2008. Supported gold nanoparticles as catalysts for organic reactions. Chem Soc Rev 37:2096–2126. https://doi.org/10.1039/b707314n.
11. Zhong CJ, Maye MM. 2001. Core-shell assembled nanoparticles as catalysts. Adv Mater 13:1507–1511.
12. Rolden Cuenya B. 2013. Metal nanoparticle catalysts beginning to shape-up. Acc Chem Res 46:1682–1691. https://doi.org/10.1021/ar300226p.
13. Thakkar KN, Mhatre SS, Parikh RY. 2010. Biological synthesis of metallic nanoparticles. Nanomed Nanotechnol Biol Med 6:257–262. https://doi.org/10.1016/j.nano.2009.07.002.
14. Ahmad A, Mukherjee P, Senapati S, Mandal D, Khan MI, Kumar R, Sastry M. 2003. Extracellular biosynthesis of silver nanoparticles using the fungus *Fusarium oxysporum*. Colloids Surf B Biointerfaces 28:313–318. https://doi.org/10.1016/S0927-7765(02)00174-1.
15. Huang J, Li Q, Sun D, Lu Y, Su Y, Yang X, Wang H, Wang Y, Shao W, He N, Hong J, Chen C. 2007. Biosynthesis of silver and gold nanoparticles by novel sundried *Cinnamomum camphora* leaf. Nanotechnology 18:105104. https://doi.org/10.1088/0957-4484/18/10/105104.
16. De Windt W, Aelterman P, Verstraete W. 2005. Bioreductive deposition of palladium (0) nanoparticles on *Shewanella oneidensis* with catalytic activity towards reductive dechlorination of polychlorinated biphenyls. Environ Microbiol 7:314–325. https://doi.org/10.1111/j.1462-2920.2005.00696.x.
17. Beeler E, Singh OV. 2016. Extremophiles as sources of inorganic bionanoparticles. World J Microbiol Biotechnol 32:156. https://doi.org/10.1007/s11274-016-2111-7.
18. Gadd GM. 2010. Metals, minerals and microbes: geomicrobiology and bioremediation. Microbiology 156:609–643. https://doi.org/10.1099/mic.0.037143-0.
19. Bauermeister A, Moeller R, Reitz G, Sommer S, Rettberg P. 2011. Effect of relative humidity on *Deinococcus radiodurans*' resistance to prolonged desiccation, heat, ionizing, germicidal, and environmentally relevant UV radiation. Microb Ecol 61:715–722. https://doi.org/10.1007/s00248-010-9785-4.
20. Slade D, Radman M. 2011. Oxidative stress resistance in *Deinococcus radiodurans*. Microbiol Mol Biol Rev 75:133–191. https://doi.org/10.1128/MMBR.00015-10.
21. Makarova KS, Aravind L, Wolf YI, Tatusov RL, Minton KW, Koonin EV, Daly MJ. 2001. Genome of the extremely radiation-resistant bacterium *Deinococcus radiodurans* viewed from the perspective of comparative genomics. Microbiol Mol Biol Rev 65:44–79. https://doi.org/10.1128/MMBR.65.1.44-79.2001.
22. Brim H, McFarlan SC, Fredrickson JK, Minton KW, Zhai M, Wackett LP, Daly MJ. 2000. Engineering *Deinococcus radiodurans* for metal remediation in radioactive mixed waste environments. Nat Biotechnol 18:85–90. https://doi.org/10.1038/71986.
23. Appukuttan D, Rao AS, Apte SK. 2006. Engineering of *Deinococcus radiodurans* R1 for bioprecipitation of uranium from dilute nuclear waste. Appl Environ Microbiol 72:7873–7878. https://doi.org/10.1128/AEM.01362-06.
24. Kulkarni R, Shaiwale N, Deobagkar DN, Deobagkar DD. 2015. Synthesis and extracellular accumulation of silver nanoparticles by employing radiation-resistant *Deinococcus radiodurans*, their characterization, and determination of bioactivity. Int J Nanomedicine 10:963–974.
25. Li J, Li Q, Ma X, Tian B, Li T, Yu J, Dai S, Weng Y, Hua Y. 2016. Biosynthesis of gold nanoparticles by the extreme bacterium *Deinococcus radiodurans* and an evaluation of their antibacterial properties. Int J Nanomedicine 11:5931–5944. https://doi.org/10.2147/IJN.S119618.
26. Kumar V, Yadav SK. 2009. Plant-mediated synthesis of silver and gold nanoparticles and their applications. J Chem Technol Biotechnol 84:151–157. https://doi.org/10.1002/jctb.2023.
27. Durán N, Marcato PD, Durán M, Yadav A, Gade A, Rai M. 2011. Mechanistic aspects in the biogenic synthesis of extracellular metal nanoparticles by peptides, bacteria, fungi, and plants. Appl Microbiol Biotechnol 90:1609–1624. https://doi.org/10.1007/s00253-011-3249-8.
28. Kalimuthu K, Suresh Babu R, Venkataraman D, Bilal M, Gurunathan S. 2008. Biosynthesis of silver nanocrystals by *Bacillus licheniformis*. Colloids Surf B Biointerfaces 65:150–153. https://doi.org/10.1016/j.colsurfb.2008.02.018.
29. Gurunathan S, Kalishwaralal K, Vaidyanathan R, Venkataraman D, Pandian SRK, Muniyandi J, Hariharan N, Eom SH. 2009. Biosynthesis, purification and characterization of silver nanoparticles using *Escherichia coli*. Colloids Surf B Biointerfaces 74:328–335. https://doi.org/10.1016/j.colsurfb.2009.07.048.
30. Riddin TL, Gericke M, Whiteley CG. 2006. Analysis of the inter- and extracellular formation of platinum nanoparticles by *Fusarium oxysporum* f. sp. *lycopersici* using response surface methodology. Nanotechnology 17:3482–3489. https://doi.org/10.1088/0957-4484/17/14/021.
31. Ramanathan R, Field MR, O'Mullane AP, Smooker PM, Bhargava SK, Bansal V. 2013. Aqueous phase synthesis of copper nanoparticles: a link between heavy metal resistance and nanoparticle synthesis ability in bacterial systems. Nanoscale 5:2300–2306. https://doi.org/10.1039/C2NR32887A.
32. Zhang C, Wei J, Zheng Z, Ying N, Sheng D, Hua Y. 2005. Proteomic analysis of *Deinococcus radiodurans* recovering from γ-irradiation. Proteomics 5:138–143. https://doi.org/10.1002/pmic.200300875.
33. Tsai C-H, Liao R, Chou B, Contreras LM. 2015. Transcriptional analysis of *Deinococcus radiodurans* reveals novel small RNAs that are differentially expressed under ionizing radiation. Appl Environ Microbiol 81:1754–1764. https://doi.org/10.1128/AEM.03709-14.
34. Gallardo OAD, Moiraghi R, Macchione MA, Godoy JA, Pérez MA, Coronado EA, Macagno VA. 2012. Silver oxide particles/silver nanoparticles interconversion: susceptibility of forward/backward reactions to the chemical environment at room temperature. RSC Adv 2:2923. https://doi.org/10.1039/c2ra01044e.
35. Qu Y, Yang H, Yang N, Fan Y, Zhu H, Zou G. 2006. The effect of reaction temperature on the particle size, structure and magnetic properties of coprecipitated $CoFe_2O_4$ nanoparticles. Mater Lett 60:3548–3552. https://doi.org/10.1016/j.matlet.2006.03.055.
36. Jiang XC, Chen WM, Chen CY, Xiong SX, Yu AB. 2011. Role of temperature in the growth of silver nanoparticles through a synergetic reduction approach. Nanoscale Res Lett 6:32.
37. Sathishkumar M, Sneha K, Won SW, Cho CW, Kim S, Yun YS. 2009. *Cinnamon zeylanicum* bark extract and powder mediated green synthesis of nano-crystalline silver particles and its bactericidal activity. Colloids Surf B Biointerfaces 73:332–338. https://doi.org/10.1016/j.colsurfb.2009.06.005.
38. Govindaraju K, Tamilselvan S, Kiruthiga V, Singaravelu G. 2010. Biogenic silver nanoparticles by *Solanum torvum* and their promising antimicrobial activity. J Biopestic 3(Special Issue):394–399.
39. Mahl D, Diendorf J, Ristig S, Greulich C, Li ZA, Farle M, Köller M, Epple M. 2012. Silver, gold, and alloyed silver-gold nanoparticles: characterization and comparative cell-biologic action. J Nanopart Res 14:1153. https://doi.org/10.1007/s11051-012-1153-5.
40. Daniel MCM, Astruc D. 2004. Gold nanoparticles: assembly, supramolecular chemistry, quantum-size related properties and applications toward biology, catalysis and nanotechnology. Chem Rev 104:293–346. https://doi.org/10.1021/cr030698+.
41. Jain PK, Lee KS, El-Sayed IH, El-Sayed MA. 2006. Calculated absorption and scattering properties of gold nanoparticles of different size, shape, and composition: applications in biological imaging and biomedicine. J Phys Chem B 110:7238–7248. https://doi.org/10.1021/jp057170o.
42. Daly MJ, Gaidamakova EK, Matrosova VY, Kiang JG, Fukumoto R, Lee DY, Wehr NB, Viteri GA, Berlett BS, Levine RL. 2010. Small-molecule antioxidant proteome-shields in *Deinococcus radiodurans*. PLoS One 5:e12570. https://doi.org/10.1371/journal.pone.0012570.
43. Anil Kumar S, Abyaneh MK, Gosavi SW, Kulkarni SK, Pasricha R, Ahmad A, Khan MI. 2007. Nitrate reductase-mediated synthesis of silver nanoparticles from $AgNO_3$. Biotechnol Lett 29:439–445. https://doi.org/10.1007/s10529-006-9256-7.
44. Hulkoti NI, Taranath TC. 2014. Biosynthesis of nanoparticles using microbes: a review. Colloids Surf B Biointerfaces 121:474–483. https://doi.org/10.1016/j.colsurfb.2014.05.027.
45. Siva Kumar K, Kumar G, Prokhorov E, Luna-Bárcenas G, Buitron G, Khanna VG, Sanchez IC. 2014. Exploitation of anaerobic enriched mixed bacteria (AEMB) for the silver and gold nanoparticles synthesis. Colloids Surfaces A Physicochem Eng Aspects 462:264–270. https://doi.org/10.1016/j.colsurfa.2014.09.021.
46. Sun Y, Xia Y. 2003. Triangular nanoplates of silver: synthesis, characterization, and use as sacrificial templates for generating triangular nanorings of gold. Adv Mater 15:695–699. https://doi.org/10.1002/adma.200304652.
47. Riddin T, Gericke M, Whiteley CG. 2010. Biological synthesis of platinum

nanoparticles: effect of initial metal concentration. Enzyme Microb Technol 46:501–505. https://doi.org/10.1016/j.enzmictec.2010.02.006.
48. Song JY, Kim BS. 2009. Rapid biological synthesis of silver nanoparticles using plant leaf extracts. Bioprocess Biosys Eng 32:79–84. https://doi.org/10.1007/s00449-008-0224-6.
49. Morones JR, Elechiguerra JL, Camacho A, Holt K, Kouri JB, Ramírez JT, Yacaman MJ. 2005. The bactericidal effect of silver nanoparticles. Nanotechnology 16:2346–2353. https://doi.org/10.1088/0957-4484/16/10/059.
50. Li T, Albee B, Alemayehu M, Diaz R, Ingham L, Kamal S, Rodriguez M, Whaley Bishnoi S. 2010. Comparative toxicity study of Ag, Au, and Ag-Au bimetallic nanoparticles on *Daphnia magna*. Anal Bioanal Chem 398:689–700. https://doi.org/10.1007/s00216-010-3915-1.
51. Pal S, Tak YK, Song JM. 2007. Does the antibacterial activity of silver nanoparticles depend on the shape of the nanoparticle? A study of the Gram-negative bacterium *Escherichia coli*. Appl Environ Microbiol 73:1712–1720. https://doi.org/10.1128/AEM.02218-06.
52. Dai Q, Lei L, Zhang X. 2008. Enhanced degradation of organic wastewater containing *p*-nitrophenol by a novel wet electrocatalytic oxidation process: parameter optimization and degradation mechanism. Sep Purif Technol 61:123–129. https://doi.org/10.1016/j.seppur.2007.10.006.
53. Gangula A, Podila R, M R, Karanam L, Janardhana C, Rao AM. 2011. Catalytic reduction of 4-nitrophenol using biogenic gold and silver nanoparticles derived from *Breynia rhamnoides*. Langmuir 27:15268–15274. https://doi.org/10.1021/la2034559.
54. Esumi K, Isono R, Yoshimura T. 2003. Preparation of silver-, platinum-, and palladium-PAMAM dendrimer nanocomposites and their catalytic activities for reduction of 4-nitrophenol. Shikizai Kyokaishi 76:421–427. (In Japanese.)
55. Kästner C, Thünemann AF. 2016. Catalytic reduction of 4-nitrophenol using silver nanoparticles with adjustable activity. Langmuir 32:7383–7391. https://doi.org/10.1021/acs.langmuir.6b01477.
56. Shankar SS, Ahmad A, Pasricha R, Sastry M. 2003. Bioreduction of chloroaurate ions by geranium leaves and its endophytic fungus yields gold nanoparticles of different shapes. J Mater Chem 13:1822–1826. https://doi.org/10.1039/b303808b.
57. Balouiri M, Sadiki M, Ibnsouda SK. 2016. Methods for in vitro evaluating antimicrobial activity: a review. J Pharm Anal 6:71–79. https://doi.org/10.1016/j.jpha.2015.11.005.
58. Zheng Z, Huang Q, Guan H, Liu S. 2015. In situ synthesis of silver nanoparticles dispersed or wrapped by a *Cordyceps sinensis* exopolysaccharide in water and their catalytic activity. RSC Adv 5:69790–69799. https://doi.org/10.1039/C5RA09452F.